nature genetics

MCT1-mediated transport of a toxic molecule is an effective strategy for targeting glycolytic tumors

Kivanç Birsoy[1–4], Tim Wang[1–4], Richard Possemato[1–4], Omer H Yilmaz[1–4], Catherine E Koch[1,2], Walter W Chen[1–4], Amanda W Hutchins[1–4], Yetis Gultekin[1–4], Tim R Peterson[1–4], Jan E Carette[1,6], Thijn R Brummelkamp[1,6], Clary B Clish[3] & David M Sabatini[1–5]

There is increasing evidence that oncogenic transformation modifies the metabolic program of cells. A common alteration is the upregulation of glycolysis, and efforts to target glycolytic enzymes for anticancer therapy are under way. Here, we performed a genome-wide haploid genetic screen to identify resistance mechanisms to 3-bromopyruvate (3-BrPA), a drug candidate that inhibits glycolysis in a poorly understood fashion. We identified the *SLC16A1* gene product, MCT1, as the main determinant of 3-BrPA sensitivity. MCT1 is necessary and sufficient for 3-BrPA uptake by cancer cells. Additionally, *SLC16A1* mRNA levels are the best predictor of 3-BrPA sensitivity and are most elevated in glycolytic cancer cells. Furthermore, forced MCT1 expression in 3-BrPA–resistant cancer cells sensitizes tumor xenografts to 3-BrPA treatment *in vivo*. Our results identify a potential biomarker for 3-BrPA sensitivity and provide proof of concept that the selectivity of cancer-expressed transporters can be exploited for delivering toxic molecules to tumors.

As a result of the rewiring of small-molecule metabolism that accompanies oncogenic transformation, cancer cells acquire metabolic liabilities not shared by their normal counterparts[1–4]. There is great interest in identifying these liabilities and exploiting them for the development of new cancer-selective therapies[5]. Many cancer cells activate aerobic glycolysis and so have high rates of glucose uptake and lactate excretion, even when oxygen is available for oxidative phosphorylation[6]. Several glycolytic enzymes, as well as the transporters that import glucose and export lactate, are considered targets for drug development[7–13]. We undertook a loss-of-function genetic screen to identify genes that affect the sensitivity of cancer cells to 3-BrPA, a drug candidate under clinical development[14,15]. 3-BrPA has cytotoxic effects and decreases cellular energy levels by inhibiting glycolysis in a poorly understood fashion[16]. In addition to targeting glycolytic enzymes[17–19], 3-BrPA can also inhibit several non-glycolytic enzymes[20–24] and, given its simple structure, is likely to have more than one direct protein target within cells. Thus, 3-BrPA is probably best characterized as a toxic molecule rather than a specific inhibitor of glycolysis. Here, we identify the *SLC16A1* gene product, monocarboxylate transporter 1 (MCT1), as the main determinant of 3-BrPA uptake and sensitivity, leading us to propose the therapeutic strategy of using MCT1-mediated transport to deliver toxic molecules to glycolytic tumors.

Gene-trap insertional mutagenesis in haploid or near-haploid metazoan cells has enabled genome-wide loss-of-function screens for genes underlying basic cellular physiology[25–27]. For example, screens in the near-haploid KBM7 human cell line identified the host factors necessary for the cytotoxic effects of several viruses and microbial toxins[28–30]. To apply this approach to the study of 3-BrPA, we used retroviral infection to create a library of mutagenized haploid KBM7 cells containing ~70 million insertions, which covered approximately 98% of all genes expressed in KBM7 cells[30]. The mutagenized cells were treated with 3-BrPA, and surviving cells were expanded as a pool. Using massively parallel sequencing, insertions in the resistant population were mapped to the human genome. Proximity index analysis was used to identify genomic regions that contained multiple gene-trap insertions in close proximity. *SLC16A1* and *BSG* (encoding basigin) were the two most frequently inactivated genes (**Fig. 1a**) and had the highest degree of insertional enrichment compared to the unselected control cells ($P = 4.7 \times 10^{-121}$ and 5×10^{-29}, respectively) (**Supplementary Fig. 1**). The highest scoring gene, *SLC16A1*, encodes MCT1, an H^+-linked monocarboxylate transporter that excretes lactate from cells and is highly upregulated in a subset of cancers[31–36]. The second highest scoring gene, *BSG*, encodes a chaperone necessary for escorting MCT1 to the plasma membrane[37,38]. To enable the in-depth study of the effects of MCT1 loss, we isolated two clones (clones A and B) that carried insertions in the first intron of the *SLC16A1* gene (**Fig. 1b**) and in which MCT1 protein was undetectable by immunoblotting (**Fig. 1c**). Consistent with the screening results, MCT1-null cells were completely resistant to doses of 3-BrPA (**Fig. 1d**) that in parental KBM7 cells induced cell death accompanied by caspase-3 activation (**Supplementary Fig. 1**). Notably, re-expression of MCT1

[1]Whitehead Institute for Biomedical Research, Cambridge, Massachusetts, USA. [2]Department of Biology, Massachusetts Institute of Technology (MIT), Cambridge, Massachusetts, USA. [3]Broad Institute, Cambridge, Massachusetts, USA. [4]David H Koch Institute for Integrative Cancer Research at MIT, Cambridge, Massachusetts, USA. [5]Howard Hughes Medical Institute, MIT, Cambridge, Massachusetts, USA. [6]Present addresses: Department of Microbiology and Immunology, Stanford University School of Medicine, Stanford, California, USA (J.E.C.) and Department of Biochemistry, Netherlands Cancer Institute, Amsterdam, The Netherlands (T.R.B.). Correspondence should be addressed to D.M.S. (sabatini@wi.mit.edu).

Received 10 July; accepted 25 October; published online 2 December 2012; doi:10.1038/ng.2471

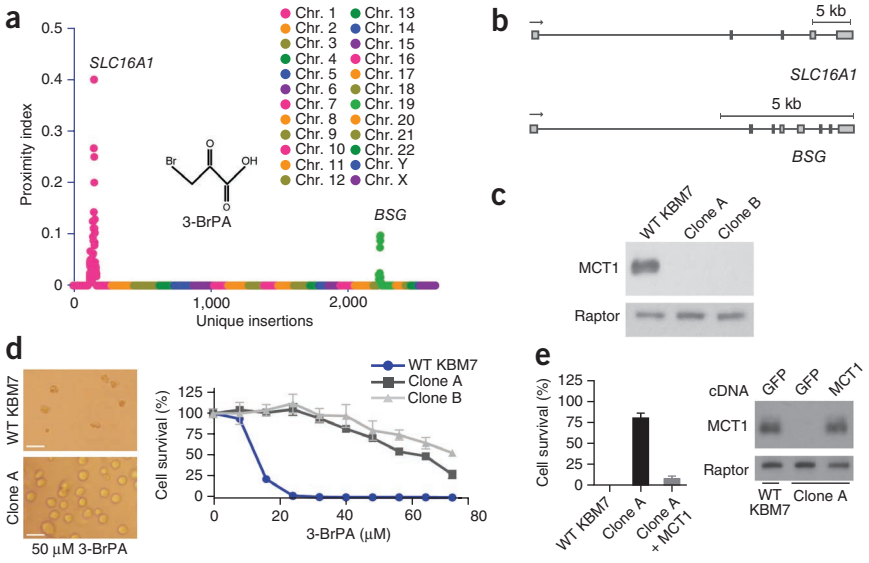

Figure 1 Haploid cell genetic screening identifies MCT1 as required for 3-BrPA sensitivity. (**a**) Mutagenized KBM7 cells were treated with 3-BrPA, and resistant clones were pooled. Gene-trap insertion sites were identified by massively parallel sequencing and mapped to the human genome. The *y* axis shows the proximity index, a measure of the local density of insertions. The *x* axis shows the insertion sites ordered by their genomic position. Inset, structure of 3-BrPA. (**b**) Map of unique insertion sites in the *SLC16A1* (encoding MCT1) and *BSG* (encoding basigin) genes in the surviving cell population. Boxes denote exons. (**c**) Immunoblotting for MCT1 protein in wild-type (WT) KBM7 cells and two clonally derived cell lines containing gene-trap insertions in *SLC16A1* (clones A and B). (**d**) Resistance of MCT1-null KBM7 clones to 3-BrPA compared to wild-type KBM7 cells. Shown are microscopic analysis (left) and survival curves (right) of wild-type and MCT1-null KBM7 cells after 3 d of 3-BrPA treatment. Scale bars, 20 μm. Error bars, s.e.m. (**e**) Exogenous expression of MCT1 in MCT1-null KBM7 cells restores their sensitivity to 3-BrPA. Shown is cell survival (left) and MCT1 expression by immunoblot (right). Error bars, s.e.m. ($n = 3$ biological replicates).

in the MCT1-null cells nearly completely restored their sensitivity to 3-BrPA (**Fig. 1e**). Thus, these data strongly point to MCT1 as an important determinant of 3-BrPA sensitivity in KBM7 cells.

To begin to understand how loss of MCT1 confers 3-BrPA resistance, we examined the effects of 3-BrPA on the metabolism of parental and MCT1-null KBM7 cells. In the absence of 3-BrPA,

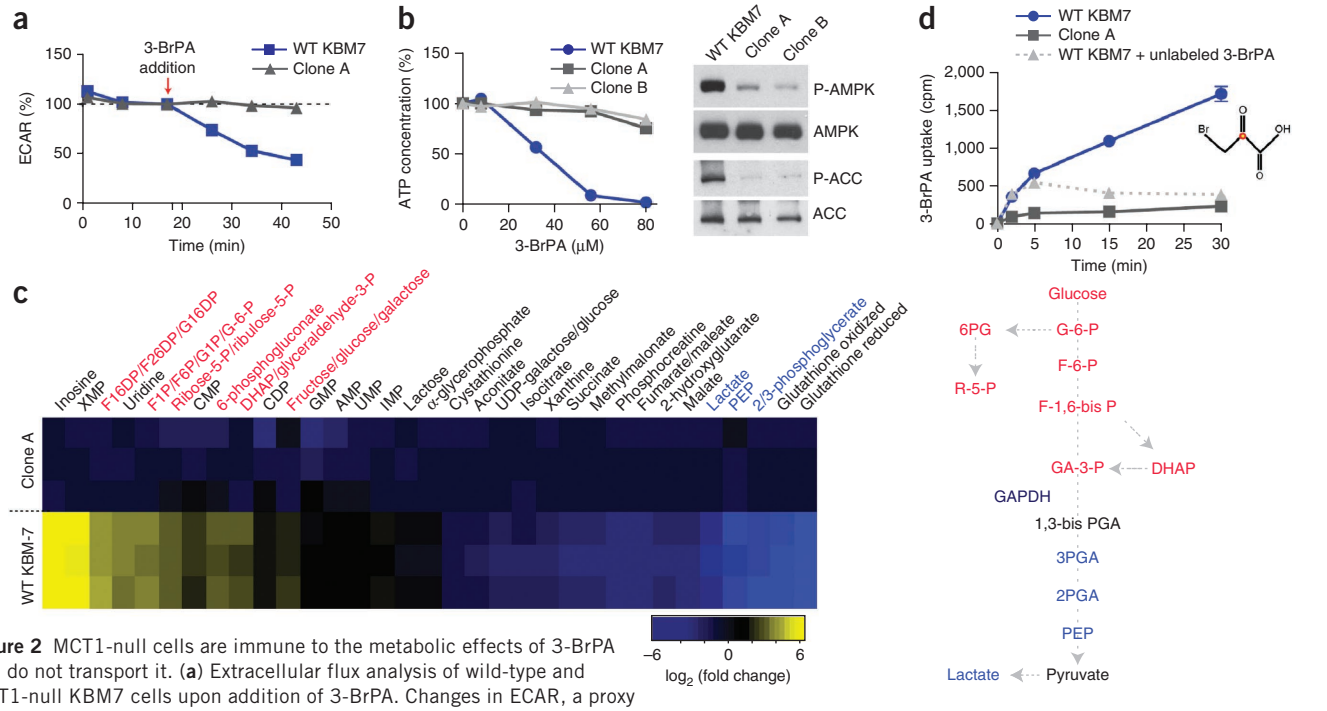

Figure 2 MCT1-null cells are immune to the metabolic effects of 3-BrPA and do not transport it. (**a**) Extracellular flux analysis of wild-type and MCT1-null KBM7 cells upon addition of 3-BrPA. Changes in ECAR, a proxy for lactate production, were monitored upon the addition of 50 μM 3-BrPA. Results are shown as a percentage of the ECAR reading immediately before 3-BrPA addition. Error bars, s.e.m. ($n = 10$). (**b**) Intracellular ATP concentration in wild-type and MCT1-null KBM7 cells were determined after treatment for 1 h with the indicated concentrations of 3-BrPA using a luciferase-based assay. Error bars, s.e.m. ($n = 6$). Immunoblots show the phosphorylation status of AMPK (P-AMPK) and ACC (P-ACC) in wild-type and MCT1-null KBM7 cells after treatment with 3-BrPA (50 μM). (**c**) Left, heatmap of relative changes in metabolite concentrations between wild-type and MCT1-null KBM7 cells upon 3-BrPA treatment. Color indicates the degree of change in metabolite abundance relative to MCT1-null KBM7 cells. Cells were cultured for 1 h with 50 μM 3-BrPA, and intracellular metabolites were obtained and analyzed by liquid chromatography–mass spectrometry (LC-MS) ($n = 3$ biological replicates). Right, schematic of the metabolites that are increased (red) or decreased (blue) in wild-type KBM7 cells compared to their MCT1-null counterparts upon 3-BrPA treatment. (**d**) [^{14}C]-labeled 3-BrPA uptake in MCT1-null and wild-type KBM7 cells in the presence or absence of excess unlabeled 3-BrPA (500 μM). Inset, structure of radioactive 3-BrPA (red dot indicates ^{14}C). Error bars, s.e.m. ($n = 3$). Note that in some instances error bars are too small for visualization or are hidden by a symbol.

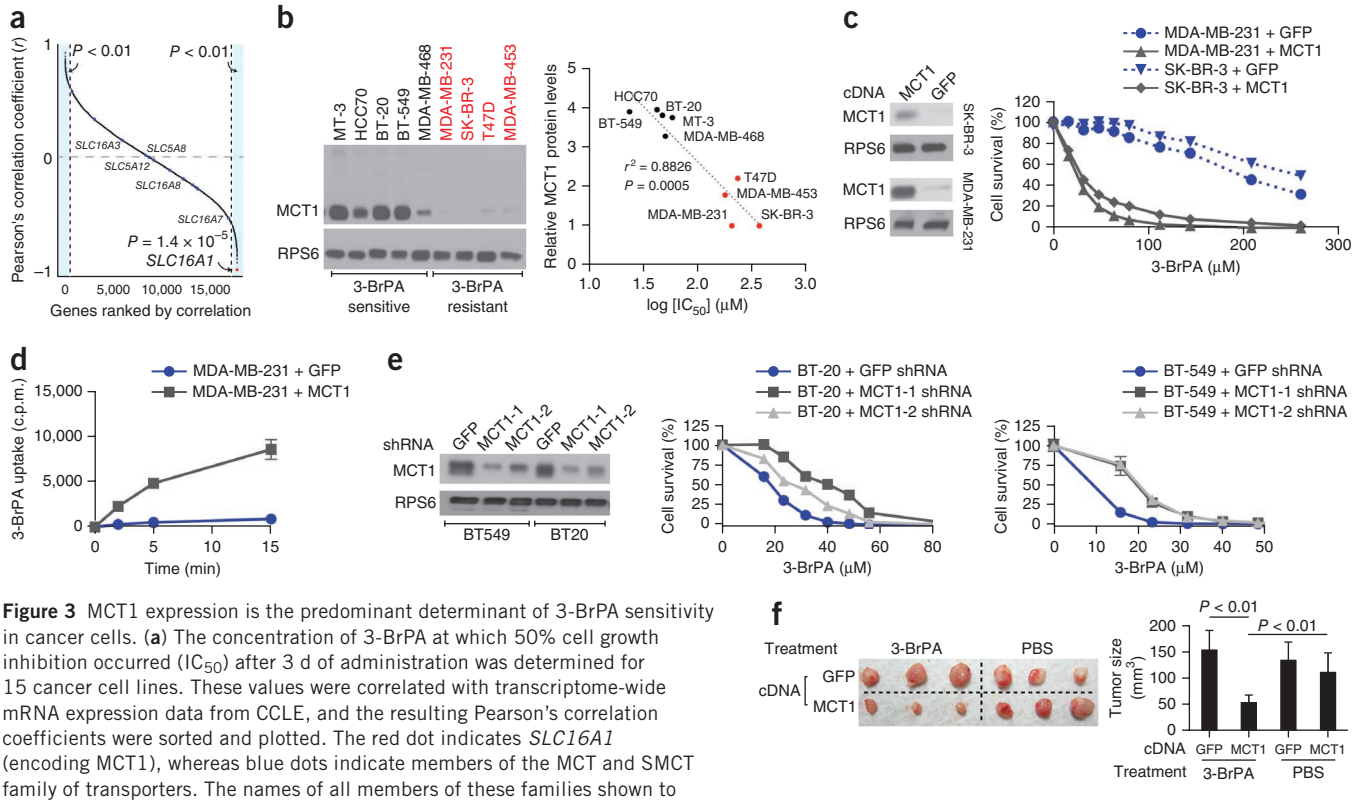

Figure 3 MCT1 expression is the predominant determinant of 3-BrPA sensitivity in cancer cells. (**a**) The concentration of 3-BrPA at which 50% cell growth inhibition occurred (IC_{50}) after 3 d of administration was determined for 15 cancer cell lines. These values were correlated with transcriptome-wide mRNA expression data from CCLE, and the resulting Pearson's correlation coefficients were sorted and plotted. The red dot indicates *SLC16A1* (encoding MCT1), whereas blue dots indicate members of the MCT and SMCT family of transporters. The names of all members of these families shown to transport lactate are indicated on the plot. (**b**) Left, immunoblot showing MCT1 protein levels for nine breast cancer cell lines. Cell lines resistant to 3-BrPA are shown in red. Right, relative protein levels correlated with the corresponding IC_{50} values for 3-BrPA for each cell line. (**c**) Left, immunoblot for MCT1 levels in SK-BR-3 and MDA-MB-231 cells expressing control GFP protein or MCT1. Right, survival curves of the indicated cell lines expressing MCT1 and treated with 3-BrPA. Error bars, s.e.m. ($n = 3$). (**d**) [^{14}C]-labeled 3-BrPA uptake in parental and MCT1-overexpressing MDA-MB-231 cells. Error bars, s.e.m. ($n = 3$). (**e**) Immunoblots (left) and survival curves (right) upon 3-BrPA treatment of the indicated cell lines expressing short hairpin RNAs (shRNAs) targeting the mRNA for control GFP protein or MCT1 (MCT1-1 and MCT1-2). Error bars, s.e.m. ($n = 3$). (**f**) Representative photographs (left) and average weights (right) of tumors formed by MDA-MB-231 cells expressing cDNA for MCT1 or GFP after 3 weeks of treatment with vehicle (PBS) or 3-BrPA (8 mg/kg). Error bars, s.d. ($n = 5$). Note that in some instances error bars are too small for visualization or are hidden by a symbol.

there was no differences in lactate production or oxygen consumption between the cell types (**Supplementary Fig. 2**), suggesting that MCT1 loss does not alter basal energy metabolism to any great extent. In contrast, 3-BrPA caused a substantial decrease in the extracellular acidification rate (ECAR), a proxy for lactate production, and total ATP levels (**Fig. 2a**,**b**) of parental but not MCT1-null KBM7 cells. Consistent with these findings, 3-BrPA did not affect AMP-activated protein kinase (AMPK) and acetyl-CoA carboxylase (ACC) phosphorylation, markers of energy deficit[39], in MCT1-null cells, whereas it robustly increased the presence of these markers in wild-type counterparts (**Fig. 2b**). To more completely characterize the metabolic state of cells in response to 3-BrPA, we metabolically profiled wild-type and MCT1-null KBM7 cells treated with 3-BrPA. Relative to MCT1-null cells, wild-type KBM7 cells treated with 3-BrPA showed an accumulation of the glycolytic intermediates that precede the synthesis of glyceraldehyde 3-phosphate, a substrate for glyceraldehyde 3-phosphate dehydrogenase (GAPDH), but a depletion of those that are synthesized later. Furthermore, 3-BrPA–treated wild-type KBM7 cells accumulated intermediates of the pentose phosphate pathway, which branches off from glycolysis above the GAPDH-mediated step (**Fig. 2c**). Additionally, the partial suppression by RNA interference (RNAi) of GAPDH expression slowed down cancer cell proliferation and sensitized cells to 3-BrPA treatment (**Supplementary Fig. 3**). 3-BrPA has previously been shown to inhibit GAPDH[17], along with several other glycolytic enzymes, including hexokinase 2 (refs. 40–42), lactate dehydrogenase[19], succinate dehydrogenase[18,43], aldolase[44] and pyruvate kinase[45,46]. However, our metabolite profiling strongly implicates GAPDH inhibition as the primary cause of the anti-glycolytic effects of 3-BrPA (**Fig. 2c**). Altogether, these data show that MCT1-null KBM7 cells are resistant to the metabolic effects of 3-BrPA, suggesting that 3-BrPA might not enter cells in the absence of MCT1 and implicating MCT1 as a 3-BrPA transporter.

Indeed, compared to parental KBM7 cells, MCT1-null cells did not take up [^{14}C]-labeled 3-BrPA (**Fig. 2d**). Unlabeled 3-BrPA and, to a lesser extent, known MCT1 substrates, such as lactate and pyruvate, effectively competed with the uptake of radiolabeled 3-BrPA, showing that transport is specific (**Supplementary Fig. 4**). Moreover, consistent with the pH dependence of MCT1-mediated transport[31,47], a reduction in extracellular pH enhanced 3-BrPA uptake (**Supplementary Fig. 4**). Thus, MCT1 is necessary for the cellular uptake of 3-BrPA and, given its capacity to transport monocarboxylates[47], probably directly transports 3-BrPA.

Considering that there are many MCTs and sodium-coupled monocarboxylate transporters (SMCTs) encoded in the human genome, we took an unbiased approach to ask whether MCT1 expression is the most predictive of 3-BrPA sensitivity. In a panel of 15 cancer cell lines, we determined half-maximal inhibitory concentration (IC_{50}) values for 3-BrPA–induced cell death and correlated them with transcriptome-wide mRNA expression data from the Cancer Cell Line Encyclopedia

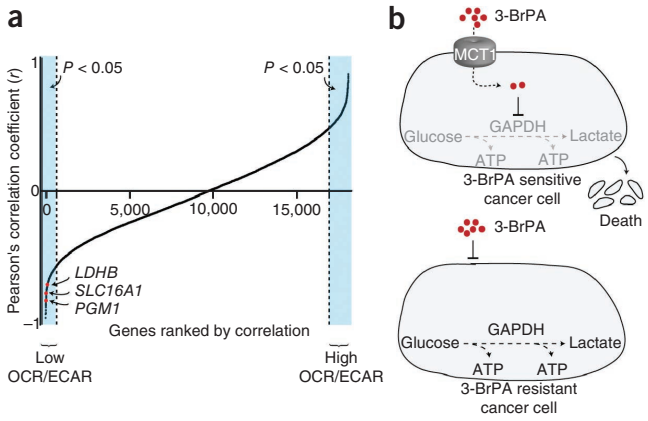

Figure 4 MCT1 expression correlates with glycolysis upregulation in cancer cells. (**a**) OCR/ECAR values were determined for 15 cell lines using the Seahorse Extracellular Flux Analyzer. These values were correlated with transcriptome-wide mRNA expression data from CCLE, and the resulting Pearson's correlation coefficients were sorted and plotted. (**b**) Schematic of the toxic cargo delivery strategy using 3-BrPA. Top, glycolytic cancer cells express high amounts of MCT1 and are sensitive to 3-BrPA. Bottom, cancer cells with low or no MCT1 are resistant to 3-BrPA.

(CCLE)[48]. Notably, of the 20,000 mRNAs examined, *SLC16A1* mRNA levels were the single best predictor of 3-BrPA sensitivity ($r = -0.89$, $P = 1.4 \times 10^{-5}$) (**Fig. 3a**). Furthermore, the expression of no other member of the MCT and SMCT monocarboxylate transporter families was significantly correlated with the 3-BrPA sensitivity of cancer cell lines (**Fig. 3a** and **Supplementary Fig. 5**). Another monocarboxylate transporter, Jen1p, was recently implicated as the primary carrier of 3-BrPA in yeast[49]; however, this transporter bears no homology to any human gene product.

We next asked whether MCT1 expression could also predict 3-BrPA sensitivity within a single cancer type, focusing on breast cancer lines because they exhibit a particularly wide range of MCT1 expression (**Supplementary Fig. 6**). Indeed, breast cancer lines with high amounts of MCT1 protein were sensitive to 3-BrPA, whereas those with low or no MCT1 expression were resistant to even high concentrations of 3-BrPA (**Fig. 3b**). Stable expression of MCT1 in two breast cancer lines with low MCT1 expression (MDA-MB-231 and SK-BR-3) was sufficient to sensitize them to 3-BrPA (**Fig. 3c**). As in KBM7 cells, MCT1 expression did not alter lactate production or oxygen consumption, but it did enhance uptake of [^{14}C]-labeled 3-BrPA (**Fig. 3d**). Conversely, the partial suppression by RNAi of MCT1 expression was sufficient to confer resistance to 3-BrPA in cell lines with high levels of MCT1 (BT-20 and BT-549) (**Fig. 3e**).

To test whether MCT1 expression could affect the sensitivity of established tumors to 3-BrPA, parental MDA-MB-231 cells, which express low levels of MCT1 (**Supplementary Fig. 6**), were injected subcutaneously into the left flanks of nude mice, while MDA-MB-231 cells stably expressing MCT1 were injected into the contralateral flanks of the same animals. We allowed palpable subcutaneous tumors to form for 2 weeks before beginning 3-BrPA administration. After 3 weeks of 3-BrPA treatment, tumors with forced MCT1 expression were significantly smaller than those that were untreated or treated with 3-BrPA but expressed control green fluorescent protein (GFP) (**Fig. 3f** and **Supplementary Fig. 6**). These results indicate that MCT1 expression is sufficient to sensitize preformed tumors to 3-BrPA treatment and has predictive value for determining 3-BrPA sensitivity *in vivo*.

We additionally examined whether cancer cells with high levels of MCT1 expression shared any metabolic properties. Using the oxygen consumption rate (OCR) to ECAR ratio as a measure of the relative contributions of oxidative phosphorylation and glycolysis to cellular energy production, we compared OCR/ECAR ratios from 15 cancer cell lines with genome-wide expression data obtained from CCLE. Notably, along with two glycolytic enzymes (LDHB and PGM1), MCT1 was among the factors whose expression most strongly and significantly correlated with lower OCR/ECAR ratios (**Fig. 4** and **Supplementary Fig. 6**). This finding indicates that tumors that have the highest rates of glycolysis are more likely to have high MCT1 expression and therefore will be more sensitive to 3-BrPA treatment (**Fig. 4**).

Our results predict that MCT1 expression will serve as a biomarker for identifying tumors likely to respond to 3-BrPA treatment[14,15]. Furthermore, as we find that MCT1 expression correlates with elevated glycolysis, it may be possible to enhance the efficacy of 3-BrPA by concomitant treatment with glycolytic inhibitors so as to exploit the high glycolytic demand of tumors and the cancer-enriched expression of MCT1. It is noteworthy that small molecule inhibitors of MCT1 that inhibit lactate export from cancer cells are in development and show promise as anticancer therapies[11,50]. Although this approach requires that MCT1 be expressed and essential for cancer cell survival[11,50], 3-BrPA treatment is distinct in that it requires only MCT1 expression to be efficacious. For example, KBM7 cells are sensitive to 3-BrPA, but complete loss of MCT1 does not affect their viability.

Our data further suggest that the toxic effect of 3-BrPA is not a result of its anti-glycolytic effect but rather its highly alkylating nature. The stringent correlation between 3-BrPA sensitivity and expression of its transporter but not that of any previously identified metabolic targets or transporters[49,51] suggests that 3-BrPA is likely nonspecifically toxic once it enters the cell. Consistent with this idea, 3-BrPA has non-glycolytic targets, such as V-ATPases[20], sarcoplasmic reticulum Ca^{2+}-ATPases (SERCAs)[24], carbonic anhydrases[52] and histone deacetylases (HDACs)[53]. Like MCT1, other transporters are also upregulated in subsets of cancers[54,55], and it therefore may be possible to develop toxic molecules that, in a fashion analogous to 3-BrPA, exploit these transporters to selectively enter and target cancer cells.

METHODS

Methods and any associated references are available in the online version of the paper.

Note: Supplementary information is available in the online version of the paper.

ACKNOWLEDGMENTS

We thank members of the Sabatini laboratory and F. Reinhardt for advice and assistance. This work was supported by grants from the US National Institutes of Health (NIH; CA103866) and the David H. Koch Institute for Integrative Cancer Research to D.M.S. and fellowships from the Jane Coffin Childs Memorial Fund to K.B. and US National Science Foundation to T.W. D.M.S. is an investigator of the Howard Hughes Medical Institute.

AUTHOR CONTRIBUTIONS

K.B. and D.M.S. conceived the project. K.B. designed and performed most experiments and data analyses, with input from D.M.S. T.W. assisted with initial experiments and data analysis. C.E.K., O.H.Y., R.P., W.W.C., Y.G. and A.W.H. assisted with experiments, and T.R.P., J.E.C. and T.R.B. assisted with haploid genetic screening. C.B.C. performed metabolite profiling and analysis. K.B. and D.M.S. wrote and edited the manuscript.

COMPETING FINANCIAL INTERESTS

The authors declare no competing financial interests.

Published online at http://www.nature.com/doifinder/10.1038/ng.2471.
Reprints and permissions information is available online at http://www.nature.com/reprints/index.html.

1. Vander Heiden, M.G. Targeting cancer metabolism: a therapeutic window opens. *Nat. Rev. Drug Discov.* **10**, 671–684 (2011).
2. Thompson, C.B. Rethinking the regulation of cellular metabolism. *Cold Spring Harb. Symp. Quant. Biol.* **76**, 23–29 (2011).
3. DeBerardinis, R.J. & Thompson, C.B. Cellular metabolism and disease: what do metabolic outliers teach us? *Cell* **148**, 1132–1144 (2012).
4. Tennant, D.A., Duran, R.V. & Gottlieb, E. Targeting metabolic transformation for cancer therapy. *Nat. Rev. Cancer* **10**, 267–277 (2010).
5. Birsoy, K., Sabatini, D.M. & Possemato, R. Untuning the tumor metabolic machine: targeting cancer metabolism: a bedside lesson. *Nat. Med.* **18**, 1022–1023 (2012).
6. Warburg, O. On respiratory impairment in cancer cells. *Science* **124**, 269–270 (1956).
7. Pelicano, H., Martin, D.S., Xu, R.H. & Huang, P. Glycolysis inhibition for anticancer treatment. *Oncogene* **25**, 4633–4646 (2006).
8. Xu, R.H. *et al.* Inhibition of glycolysis in cancer cells: a novel strategy to overcome drug resistance associated with mitochondrial respiratory defect and hypoxia. *Cancer Res.* **65**, 613–621 (2005).
9. Sonveaux, P. *et al.* Targeting lactate-fueled respiration selectively kills hypoxic tumor cells in mice. *J. Clin. Invest.* **118**, 3930–3942 (2008).
10. Vander Heiden, M.G. *et al.* Identification of small molecule inhibitors of pyruvate kinase M2. *Biochem. Pharmacol.* **79**, 1118–1124 (2010).
11. Le Floch, R. *et al.* CD147 subunit of lactate/H^+ symporters MCT1 and hypoxia-inducible MCT4 is critical for energetics and growth of glycolytic tumors. *Proc. Natl. Acad. Sci. USA* **108**, 16663–16668 (2011).
12. Wood, T.E. *et al.* A novel inhibitor of glucose uptake sensitizes cells to FAS-induced cell death. *Mol. Cancer Ther.* **7**, 3546–3555 (2008).
13. Stein, M. *et al.* Targeting tumor metabolism with 2-deoxyglucose in patients with castrate-resistant prostate cancer and advanced malignancies. *Prostate* **70**, 1388–1394 (2010).
14. Pedersen, P.L. 3-bromopyruvate (3BP) a fast acting, promising, powerful, specific, and effective "small molecule" anti-cancer agent taken from labside to bedside: introduction to a special issue. *J. Bioenerg. Biomembr.* **44**, 1–6 (2012).
15. Ko, Y.H. *et al.* A translational study "case report" on the small molecule "energy blocker" 3-bromopyruvate (3BP) as a potent anticancer agent: from bench side to bedside. *J. Bioenerg. Biomembr.* **44**, 163–170 (2012).
16. Shoshan, M.C. 3-bromopyruvate: targets and outcomes. *J. Bioenerg. Biomembr.* **44**, 7–15 (2012).
17. Ganapathy-Kanniappan, S. *et al.* Glyceraldehyde-3-phosphate dehydrogenase (GAPDH) is pyruvylated during 3-bromopyruvate mediated cancer cell death. *Anticancer Res.* **29**, 4909–4918 (2009).
18. Pereira da Silva, A.P. *et al.* Inhibition of energy-producing pathways of HepG2 cells by 3-bromopyruvate. *Biochem. J.* **417**, 717–726 (2009).
19. Dell'Antone, P. Targets of 3-bromopyruvate, a new, energy depleting, anticancer agent. *Med. Chem.* **5**, 491–496 (2009).
20. Dell'Antone, P. Inactivation of H^+-vacuolar ATPase by the energy blocker 3-bromopyruvate, a new antitumour agent. *Life Sci.* **79**, 2049–2055 (2006).
21. Blessinger, K.J. & Tunnicliff, G. Kinetics of inactivation of 4-aminobutyrate aminotransferase by 3-bromopyruvate. *Biochem. Cell Biol.* **70**, 716–719 (1992).
22. Tunnicliff, G. & Ngo, T.T. Mechanism of inactivation of brain glutamic decarboxylase by 3-bromopyruvate. *Int. J. Biochem.* **9**, 249–252 (1978).
23. Arendt, T., Schugens, M.M. & Marchbanks, R.M. Reversible inhibition of acetylcholine synthesis and behavioural effects caused by 3-bromopyruvate. *J. Neurochem.* **55**, 1474–1479 (1990).
24. Jardim-Messeder, D., Camacho-Pereira, J. & Galina, A. 3-bromopyruvate inhibits calcium uptake by sarcoplasmic reticulum vesicles but not SERCA ATP hydrolysis activity. *Int. J. Biochem. Cell Biol.* **44**, 801–807 (2012).
25. Carette, J.E. *et al.* Haploid genetic screens in human cells identify host factors used by pathogens. *Science* **326**, 1231–1235 (2009).
26. Layton, J.E. Undertaking a successful gynogenetic haploid screen in zebrafish. *Methods Mol. Biol.* **546**, 31–44 (2009).
27. Elling, U. *et al.* Forward and reverse genetics through derivation of haploid mouse embryonic stem cells. *Cell Stem Cell* **9**, 563–574 (2011).
28. Carette, J.E. *et al.* Ebola virus entry requires the cholesterol transporter Niemann-Pick C1. *Nature* **477**, 340–343 (2011).
29. Guimaraes, C.P. *et al.* Identification of host cell factors required for intoxication through use of modified cholera toxin. *J. Cell Biol.* **195**, 751–764 (2011).
30. Carette, J.E. *et al.* Global gene disruption in human cells to assign genes to phenotypes by deep sequencing. *Nat. Biotechnol.* **29**, 542–546 (2011).
31. Morris, M.E. & Felmlee, M.A. Overview of the proton-coupled MCT (SLC16A) family of transporters: characterization, function and role in the transport of the drug of abuse γ-hydroxybutyric acid. *AAPS J.* **10**, 311–321 (2008).
32. Pinheiro, C. *et al.* Monocarboxylate transporter 1 is up-regulated in basal-like breast carcinoma. *Histopathology* **56**, 860–867 (2010).
33. Pinheiro, C. *et al.* Monocarboxylate transporters 1 and 4 are associated with CD147 in cervical carcinoma. *Dis. Markers* **26**, 97–103 (2009).
34. Mathupala, S.P., Parajuli, P. & Sloan, A.E. Silencing of monocarboxylate transporters via small interfering ribonucleic acid inhibits glycolysis and induces cell death in malignant glioma: an *in vitro* study. *Neurosurgery* **55**, 1410–1419 discussion 1419 (2004).
35. Koukourakis, M.I., Giatromanolaki, A., Bougioukas, G. & Sivridis, E. Lung cancer: a comparative study of metabolism related protein expression in cancer cells and tumor associated stroma. *Cancer Biol. Ther.* **6**, 1476–1479 (2007).
36. Pinheiro, C. *et al.* Increased expression of monocarboxylate transporters 1, 2, and 4 in colorectal carcinomas. *Virchows Arch.* **452**, 139–146 (2008).
37. Poole, R.C. & Halestrap, A.P. Interaction of the erythrocyte lactate transporter (monocarboxylate transporter 1) with an integral 70-kDa membrane glycoprotein of the immunoglobulin superfamily. *J. Biol. Chem.* **272**, 14624–14628 (1997).
38. Kirk, P. *et al.* CD147 is tightly associated with lactate transporters MCT1 and MCT4 and facilitates their cell surface expression. *EMBO J.* **19**, 3896–3904 (2000).
39. Mihaylova, M.M. & Shaw, R.J. The AMPK signalling pathway coordinates cell growth, autophagy and metabolism. *Nat. Cell Biol.* **13**, 1016–1023 (2011).
40. Rodrigues-Ferreira, C., da Silva, A.P. & Galina, A. Effect of the antitumoral alkylating agent 3-bromopyruvate on mitochondrial respiration: role of mitochondrially bound hexokinase. *J. Bioenerg. Biomembr.* **44**, 39–49 (2012).
41. Ko, Y.H. *et al.* Advanced cancers: eradication in all cases using 3-bromopyruvate therapy to deplete ATP. *Biochem. Biophys. Res. Commun.* **324**, 269–275 (2004).
42. Ko, Y.H., Pedersen, P.L. & Geschwind, J.F. Glucose catabolism in the rabbit VX2 tumor model for liver cancer: characterization and targeting hexokinase. *Cancer Lett.* **173**, 83–91 (2001).
43. Sanborn, B.M., Felberg, N.T. & Hollocher, T.C. The inactivation of succinate dehydrogenase by bromopyruvate. *Biochim. Biophys. Acta* **227**, 219–231 (1971).
44. Meloche, H.P., Luczak, M.A. & Wurster, J.M. The substrate analog, bromopyruvate, as both a substrate and alkylating agent for 2-keto-3-deoxy-6-phosphogluconic aldolase. Kinetic and stereochemical studies. *J. Biol. Chem.* **247**, 4186–4191 (1972).
45. Yun, S.L. & Suelter, C.H. Modification of yeast pyruvate kinase by an active site–directed reagent, bromopyruvate. *J. Biol. Chem.* **254**, 1811–1815 (1979).
46. Acan, N.L. & Ozer, N. Modification of human erythrocyte pyruvate kinase by an active site–directed reagent: bromopyruvate. *J. Enzyme Inhib.* **16**, 457–464 (2001).
47. Halestrap, A.P. The monocarboxylate transporter family—structure and functional characterization. *IUBMB Life* **64**, 1–9 (2012).
48. Barretina, J. *et al.* The Cancer Cell Line Encyclopedia enables predictive modelling of anticancer drug sensitivity. *Nature* **483**, 603–607 (2012).
49. Lis, P. *et al.* Transport and cytotoxicity of the anticancer drug 3-bromopyruvate in the yeast *Saccharomyces cerevisiae*. *J. Bioenerg. Biomembr.* **44**, 155–161 (2012).
50. Murray, C.M. *et al.* Monocarboxylate transporter MCT1 is a target for immunosuppression. *Nat. Chem. Biol.* **1**, 371–376 (2005).
51. Queirós, O. *et al.* Butyrate activates the monocarboxylate transporter MCT4 expression in breast cancer cells and enhances the antitumor activity of 3-bromopyruvate. *J. Bioenerg. Biomembr.* **44**, 141–153 (2012).
52. Göthe, P.O. & Nyman, P.O. Inactivation of human erythrocyte carbonic anhydrases by bromopyruvate. *FEBS Lett.* **21**, 159–164 (1972).
53. Thangaraju, M. *et al.* Transport by SLC5A8 with subsequent inhibition of histone deacetylase 1 (HDAC1) and HDAC3 underlies the antitumor activity of 3-bromopyruvate. *Cancer* **115**, 4655–4666 (2009).
54. Ganapathy, V., Thangaraju, M. & Prasad, P.D. Nutrient transporters in cancer: relevance to Warburg hypothesis and beyond. *Pharmacol. Ther.* **121**, 29–40 (2009).
55. Gupta, N. *et al.* Upregulation of the amino acid transporter $ATB^{0,+}$ (SLC6A14) in colorectal cancer and metastasis in humans. *Biochim. Biophys. Acta* **1741**, 215–223 (2005).

ONLINE METHODS

Materials. Antibody to MCT1 was from Millipore (ab3538p), antibody to GAPDH was from Sigma (G9545), antibodies to RPS6 (2217), ACC (3662), AMPK (2532), phosphorylated ACC (3661), phosphorylated AMPK (2535) and raptor (2280) were from Cell Signaling Technology, and horseradish peroxidase (HRP)-conjugated secondary antibody to rabbit was from Santa Cruz Biotechnology. Lactate dehydrogenase was from Roche, lactic acid and 3-BrPA were from Acros Organics, RPMI-1640 medium, glycine buffer solution, pyruvate, l-lactate, D-lactate, puromycin and polybrene were from Sigma, blasticidin was from Invivogen, [^{14}C]-labeled 3-BrPA was from Moravek Biosciences, Matrigel and Cell-Tak were from BD Biosciences, and IMDM was from US Biologicals. Cell lines were obtained from the American Type Culture Collection (ATCC). Lentiviral shRNAs were obtained from The RNAi Consortium (TRC) collection of the Broad Institute. The TRC numbers for the shRNAs used are TRCN0000072186 (GFP), TRCN0000038339 (MCT1-1), TRCN0000038340 (MCT1-2), TRCN0000221345 (GAPDH-1) and TRCN0000221346 (GAPDH-2). Primer sequences for cloning the cDNA for MCT1 into pMXs-IRES-blasticidin and pLJM1-puro are provided in **Supplementary Table 1**.

Cell culture and virus transduction. KBM7 cells were cultured in IMDM supplemented with 10% heat-inactivated FBS and penicillin-streptomycin. All other cell lines in this study were cultured in RPMI supplemented with 10% FBS. KBM7, MDA-MB-231 and SK-BR-3 cell lines stably overexpressing human MCT1 or GFP were generated by infection with lentiviruses expressing the corresponding cDNAs and were selected for blasticidin (10 μg/ml) or puromycin (4 μg/ml) resistance for 3 d, respectively. Similarly BT-20, KBM7, MDA-MB-468 and BT-549 cells expressing shRNAs to reduce MCT1 and GAPDH expression were generated by infection with lentiviruses expressing the corresponding shRNAs (**Supplementary Table 1**) and were spin infected via a 30-min spin at 1,000*g* in medium containing 4 μg/ml polybrene. Cells were next selected with puromycin.

Haploid cell screening. A haploid cell genetic screen with 3-BrPA was performed using 100 million mutagenized KBM7 cells, as described previously[30]. Mutagenized haploid KBM7 cells were exposed to 50 μM 3-BrPA for 3 weeks. Surviving clones were harvested, genomic DNA was isolated and insertions were amplified. The sequences flanking retroviral insertion sites were mapped to the human genome using inverse PCR followed by Illumina sequencing. Genomic regions with a high density of insertions were identified using the proximity index for a given insertion. Additionally, the statistical enrichment of insertions at a given locus in the selected population was calculated by comparing the number of inactivating insertions to those in the untreated control data set via Fisher's exact test. Individual clones were isolated, and genomic DNA for individually selected clones was isolated using a genomic DNA isolation kit (Qiagen). Genomic insertions were identified by inverse PCR and subsequent sequencing, as described previously[25].

Metabolic assays. The bioenergetic profiles of KBM7 and MDA-MB-231 cells in response to 3-BrPA were determined using a Seahorse Bioscience XF24 Extracellular Flux Analyzer. For the indicated experiments, 250,000 KBM7 or 40,000 MDA-MB-231 cells were seeded in Seahorse tissue culture plates using unbuffered RPMI (10 mM glucose). KBM7 cells were attached to the plates using Cell-Tak (Clontech) 1 h before the start of the experiment. For AUC (area under the curve), OCR and ECAR measurements, three consecutive readings were performed for each cell line. For experiments where 3-BrPA was used, after three consecutive readings, 50 μM 3-BrPA was injected through port A, and ECAR and OCR levels were measured. Lactate production was measured as described previously[56]. For ATP assays, 20,000 cells were seeded and treated for 1 h with the indicated amounts of 3-BrPA, and relative ATP concentrations compared to those of untreated cells were determined using a luciferase-based assay (Promega). For metabolite concentration measurements, 10 million wild-type and MCT1-null KBM7 cells were cultured for 1 h in the presence of 50 μM 3-BrPA before metabolite extraction. Then, cells were rapidly washed three times with cold PBS, and metabolites were extracted by the addition of 80% ice-cold methanol after incubation on dry ice for 15 min. Endogenous metabolite profiles were obtained using LC-MS as described[57]. Metabolite levels (n = 3 biological replicates) were normalized to cell number.

3-BrPA uptake assay. Wild-type KBM7 and MCT1-null cells were seeded in HBSS and exposed for up to 20 min to 100 μM [^{14}C]-labeled 3-BrPA (6.8 mCi/mmole) (Moravek) with or without competitor molecules, such as 3-BrPA, pyruvate, L-lactate and D-lactate. Cells were washed with cold HBSS (Invitrogen, 14025-092) and lysed in a NaOH buffer, and uptake was measured using a liquid scintillation counter.

Cell survival assays. Cells (5,000–20,000) were seeded in 96-well plates and treated with the indicated amounts of 3-BrPA. After 3 d of treatment, CellTiter-Glo (Promega) and/or CyQuant (Invitrogen) were used to measure cell cycle arrest or the percentage of cell death for each concentration compared to untreated cells. Fluorescence-activated cell sorting (FACS) analysis with Annexin V and 7-AAD staining was performed according to the manufacturer's manual (BD Pharmingen).

Correlation analysis. Fifteen cell lines (BT-474, BT-549, CAKI-1, CAL-51, HCC-70, Hs 578T, Jurkat, MDA-MB-157, MDA-MB-231, MDA-MB-453, MDA-MB-468, PC-3, SK-BR-3, T47D and ZR-75-1) were treated with 3-BrPA (0–300 μM). After 3 d, cell viability was quantified via CellTiter-Glo assay, and IC_{50} values were interpolated from the resulting dose-response curve using a nonlinear regression model. Transcriptome-wide normalized mRNA levels from gene expression profiling experiments performed on the Affymetrix Human Genome U133 Plus 2.0 chip were obtained from CCLE for all 15 cell lines. The mRNA expression pattern across all 15 samples for each of the genes was then correlated with the IC_{50} values. A similar correlation analysis was performed using OCR/ECAR values for each cell line.

Immunoblotting and immunohistochemistry. Briefly, cells were rinsed twice in ice-cold PBS and harvested in a standard lysis buffer containing 50 mM HEPES, pH 7.4, 40 mM NaCl, 2 mM EDTA, 1.5 mM orthovanadate, 50 mM NaF, 10 mM pyrophosphate, 10 mM glycerophosphate, protease inhibitors (Roche) and 1% Triton X-100. Proteins from total lysates were resolved by 8–12% SDS-PAGE and analyzed by immunoblotting using the indicated antibodies (at a 1:1,000 dilution)[56]. For quantitation, ImageJ software was used, and signals were normalized using an equal loading control (RPS6 or raptor). Immunohistochemistry was performed on formalin-fixed paraffin-embedded sections using a boiling antigen retrieval method (Dako). A 1:500 dilution of the antibody to MCT1 was used for staining.

Mouse studies. All animal studies and procedures were approved by the MIT Institutional Animal Care and Use Committee. Nude mice (Taconic) at 6–10 weeks of age were used to generate all xenografts. For subcutaneous xenografts, mice were injected at two sites in the dorsal region, under isofluorane anesthesia with 100 μl per injection of tumor cell suspension in RPMI with 20% Matrigel. For each injection, 2.5 million MDA-MB-231 cells were used. After 2 weeks, tumors were measured, and mice were separated for PBS and 3-BrPA treatment (8 mg/kg). After 3 weeks, tumors were harvested, their dimensions were measured with a caliper and tumor volume was estimated according to the formula ($0.5 \times L \times W \times W$, where L is the length and W is the width of a tumor). Tumors were fixed in formalin for later processing.

56. Possemato, R. *et al.* Functional genomics reveal that the serine synthesis pathway is essential in breast cancer. *Nature* **476**, 346–350 (2011).
57. Finley, L.W. *et al.* Skeletal muscle transcriptional coactivator PGC-1α mediates mitochondrial, but not metabolic, changes during calorie restriction. *Proc. Natl. Acad. Sci. USA* **109**, 2931–2936 (2012).